Article

Aldol condensation of cyclopentanone on hydrophobized MgO. Promotional role of water and changes in rate-limiting step upon organosilane functionalization

Duong T Ngo, Qiaohua Tan, Bin Wang, and Daniel E. Resasco

ACS Catal., **Just Accepted Manuscript** • DOI: 10.1021/acscatal.8b05103 • Publication Date (Web): 14 Feb 2019

Aldol Condensation of Cyclopentanone on Hydrophobized MgO. Promotional Role of Water and Changes in Rate-Limiting Step upon Organosilane Functionalization

Duong T. Ngo, Qiaohua Tan, Bin Wang, Daniel E. Resasco*

School of Chemical, Biological and Materials Engineering, University of Oklahoma, Norman, Oklahoma 73019, USA

* Corresponding Author:

Daniel E. Resasco Phone: (405) 325-4370

E-mail: resasco@ou.edu

Abstract

Aldol condensation is a key C-C coupling reaction for upgrading of biomass-derived oxygenates to fuels and chemicals. Here, we investigate the effects of added water on the condensation of cyclopentanone (CPO) on hydrophobized MgO catalysts. We have found that the role of water strongly depends on the degree of hydrophobic functionalization of the MgO surface. That is, on a non-functionalized (hydrophilic) high-surface-area MgO catalyst, the rate decreases with the addition of water, mostly due to active site blockage. By contrast, on MgO hydrophobized via silylation with octadecyltrichlorosilane (OTS), the rate actually increases with added water. A concomitant change in kinetics is observed from the pristine (hydrophilic) MgO to the hydrophobized sample. Specifically, on the hydrophilic sample, the reaction is first-order, as expected if the rate-limiting step is the formation of an enolate intermediate via α-H abstraction at a basic site, as widely reported in previous literature. By contrast, on the hydrophobized sample the reaction becomes second-order, indicating a shift in rate-limiting step to the bimolecular C-C coupling. On pristine MgO, acid-base pairs are fully available on the surface, with the acid site polarizing the C=O group in the second cyclopentanone (electrophile) and making the attack by the enolate very favorable. It is proposed here that grafted OTS molecules interfere between active sites, making the adsorbate-adsorbate interaction on the surface less likely and reducing the rate of C-C coupling. Both isotope effect experiments and *ab initio* molecular dynamics simulations of cyclopentanone adsorption at the MgO/OTS interface further support this argument. Therefore, the promotional role of water seems to be the assistance of the C-C bond-forming step. It is proposed that, at low concentrations, water can help the second molecule (electrophile) be polarized from a remote Mg^{2+} site through a chain of H-bonded molecules.

Keywords

aldol condensation; cyclopentanone; magnesium oxide; silane functionalization;

rate-limiting steps; α-H abstraction, C-C coupling, water promotion

1. Introduction

Staged thermal pyrolysis is one of the most promising approaches to decompose biomass into separate streams, more amenable for subsequent catalytic upgrading to fuels and chemicals.[1–6] Furanic compounds obtained from thermal decomposition in the medium range are particularly suited for C-C coupling upgrading.[2,7–10] Furfural – a representative molecule of this stage – is unstable and may easily polymerize and form humins. Then, it would be a good strategy to convert furfural to more stable cyclopentanone via a two-step metal-catalyzed aqueous hydrogenation/isomerization known as the Piancatelli ring rearrangement.[11] Subsequently, cyclopentanone can readily undergo aldol condensations to generate α,β-unsaturated dimeric ketones, followed by hydrodeoxygenation into fuel-range molecules.[12,13]

It is well known that aldol condensation is effectively catalyzed by solid bases (e.g. MgO) under water-free conditions.[14–16] To improve its surface area, MgO can be prepared via the nitrate-citrate combustion method, which renders a material with a high density of basic sites.[17,18] However, in the liquid phase this material deactivates rapidly due to accumulation of over-condensates and water produced *in situ*. In a recent study,[19] we emphasized that water is ubiquitous in biomass upgrading processes, and consequently we developed a method to improve the resistance of these catalysts to water. We found that deactivation is greatly reduced by functionalizing the surface with an alkylsilane (e.g. OTS) on both pure MgO and an MgO-SiO_2 solid mixture. Despite exhibiting a much lower basic density and lower TOF, the functionalized MgO catalysts showed ability to operate for many hours with practically no deactivation. As the hydrophobic OTS molecules inhibit the formation of an *in situ* water layer on MgO surface, a sizeable amount of active sites remained accessible for cyclopentanone to generate enolates, essentially indefinitely. In addition, OTS-functionalized MgO remarkably resisted the attack by added water.

Rate-enhancing by the presence of water is a less common phenomenon that has been observed in some reactions, such as the Fischer-Tropsch synthesis (FTS). For example, a study of Co-catalyzed FTS[20] has shown that water co-fed in the vapor phase hinders chain termination

via H-abstraction at internal positions of alkyl chains and secondary olefin isomerization. Moreover, Shi *et al.*[21] have found that the presence of a condensed aqueous phase further improves the FTS catalytic activity and the C_5-C_{20} fraction over Ru/CNT-Al_2O_3-MgO by mediating H-shuttling and facilitating CO cleavage. In addition to FTS, hydrogenation in the presence of liquid water also results in enhanced conversion with respect to the reaction in organic solvents. For example, hydrogenation of ketones on Ru is enhanced in aqueous phase by a direct involvement of water.[22] That is, water stabilization of chemisorbed species (reactants, intermediates and transition states) via H-bonding networks can effectively accelerate rate-limiting steps.[22-24] Other rate-enhancement examples involve improved solvation[25,26] and selective oxidation of surface species.[27–30] However, despite some additional examples of rate-enhancement by water,[31–35] rate-inhibition is far more usual,[36–43] with competitive adsorption and site blockage as the most common observation.[44–46]

In our previous study,[19] a drastic drop in activity was observed following the exposure of the non-functionalized MgO catalyst to 2 mL of external water, which was in excess of the amount needed to form an aqueous liquid phase. We concluded that pure MgO lost most of its active sites due to the formation of inactive layers of $Mg(OH)_2$. By contrast, the OTS-functionalized MgO sample retained most of its initial activity for several hours in the presence of excess amounts of water.[47,48] In this case, water formed droplets away from the catalyst surface rather than a layer covering the surface, which greatly delayed deactivation. In other words, functionalization with organosilanes did not eliminate water susceptibility but instead alleviated this issue to prolong material stability. No rate improvements were observed in that study due to the excess amount of water used in the experiments.

In this contribution, we report that by exposing both MgO and its OTS-modified versions to varying amounts of water significant different trends are observed. Specifically, we have found find that on the hydrophilic MgO, the reaction is first-order as expected if the rate-limiting step is the formation of an enolate intermediate via α-H abstraction at a basic site, while on the hydrophobized sample the reaction becomes second-order, indicating a shift in rate-limiting step to the bimolecular C-C coupling. It is proposed here that grafted OTS molecules interfere between active sites, making the adsorbate-adsorbate interaction on the surface less

likely and reducing the rate of C-C coupling. *Ab initio* molecular dynamics simulations of cyclopentanone adsorption at the MgO/OTS interface further support this argument. Therefore, the promotional role of water, only observed on the functionalized samples, seems to be the assistance of the C-C bond-forming step.

2. Experimental

2.1. Synthesis of catalytic materials

2.1.1. MgO-NC

MgO-NC was synthesized via nitrate-citrate combustion, the method described elsewhere.[19] Briefly, 25.6 g of $Mg(NO_3)_2.6H_2O$ (Aldrich, 99.9%, 0.1 mol) was mixed with 30 mL of water and stirred vigorously for 15 mins at 80°C. Then, a 20-mL water solution containing 19.2 g of citric acid (Aldrich, 99.5%, 0.1 mol) was added into the mixture. The resulting solution was continuously heated and stirred until half of the liquid vaporized, leaving a viscous gel. This gel was calcined overnight under static air at 550°C to obtain a high-surface-area MgO solid named MgO-NC (for nitrate-citrate combustion).

2.1.2. Octadecyltrichlorosilane-functionalized MgO

The as-prepared MgO-NC was then hydrophobized, starting with the dropwise addition of 0.45 mL of water onto 1 g of MgO-NC. The wetted material was suspended in a 1:50 v/v OTS-toluene solution.[19,49] The suspension was shaken vigorously for 10 mins, stirred overnight at room temperature, centrifuged and washed thrice with ethanol. The separated solid was dried overnight at 110°C to yield the OTS-functionalized MgO, in which OTS molecules displaced silanol groups to generate a hydrophobic surface. Materials synthesized from this method were generalized as MgO(x)-OTS(y). Such denotation means a catalyst nominally containing x wt.% of MgO and y wt.% of OTS.

2.1.3. Removal of the alkyl chains of MgO-OTS by oxidation

The as-prepared MgO(70)-OTS(30) was calcined under a temperature program for complete combustion of octadecyl groups. In details, a calculated amount of MgO(70)-OTS(30) was placed in the middle of a glass tube. Both ends of the tube were packed with glass

wool. The tube was then horizontally connected to a furnace and applied with a 40-sccm air flow at room temperature. MgO(70)-OTS(30) was first heated to 300°C under a ramp rate of 1°C.min^{-1}. The temperature was stabilized at 300°C for 1 hour before increased to 450°C under the same ramp rate. The sample was maintained at 450°C for 4 hours, then cooled down overnight and finally collected. The obtained solid was denoted as MgO(70)-OTS(30) PC. PC here stands for post-calcination, as this solid was prepared through thermal removal of the alkyl chains of MgO(70)-OTS(30).

2.2. Characterization

2.2.1. Surface density of functional groups (OTS per nm^2)

To quantify the surface density of OTS functionalities in terms of molecules per nm^2 the following data were obtained from TGA and BET measurements. First, the total content of OTS in the functionalized MgO sample was determined by thermogravimetric analysis (TGA). In this measurement, a known amount of functionalized sample was analyzed by heating under flow of an Ar-air mixture in a linear ramp of 2°C.min^{-1} starting at 40°C described elsewhere.[19] The specific surface areas for the various samples were obtained on a Micromeritics 2010 instrument. Assuming complete hydrolysis of the chloro-groups in OTS and simplifying the analysis considering only monodentate anchoring, we calculate:

$$x = \frac{n_{OTS} \times N_A}{A_{MgO\text{-}NC}} = \frac{\frac{m_{C_{18}H_{37}Si(OH)_2O\text{-}}}{MW_{C_{18}H_{37}Si(OH)_2O\text{-}}} \times N_A}{m_{MgO\text{-}NC} \times S_{BET\ MgO\text{-}NC}}$$

or

$$x = \frac{\frac{m_{C_{18}H_{37}Si(OH)_2O\text{-}}}{MW_{C_{18}H_{37}Si(OH)_2O\text{-}}} \times N_A}{(1 - m_{C_{18}H_{37}Si(OH)_2O\text{-}}) \times S_{BET\ MgO\text{-}NC}}$$

where x is the number of molecules of OTS (actually $C_{18}H_{37}Si(OH)_2O$-), anchored per unit area of MgO-NC in MgO(70)-OTS(30); $m_{C_{18}H_{37}Si(OH)_2O\text{-}}$ is the TGA-based content of OTS in MgO(70)-OTS(30) [g.g catalyst^{-1}]; $m_{MgO\text{-}NC}$ is the TGA-based content of MgO-NC in MgO(70)-OTS(30) [g.g catalyst^{-1}].

2.2.2. CO_2-TPD

The densities of basic sites for MgO(70)-OTS(30), MgO(70)-OTS(30) PC and MgO(85)-OTS(15) were quantified via temperature-programmed desorption (TPD) of adsorbed CO_2 following the method described elsewhere.[50] The CO_2-TPD of MgO-NC reported before[19] was used as a reference. Analogous to the method described elsewhere,[19] 100 mg of catalyst was heated to 200°C in the TPD system with a heating ramp of 10°C.min^{-1}, under He flow rate of 30 mL.min^{-1} and then cooled down to room temperature. A CO_2 flow rate of 30 mL.min^{-1} was passed through the sample for 30 mins, followed by a 2-hour purge with He to remove any physisorbed CO_2. The TPD was performed under the same He flow rate by heating to 600°C with a heating ramp of 10°C.min^{-1}.

2.3. Catalytic measurements

2.3.1. Reactor operating conditions and analysis methods

Aldol condensation of cyclopentanone (CPO) was conducted under N_2 atmosphere following the same reaction system and procedure as described before.[19] Briefly, for each run, a cyclohexane solvent-catalyst mixture was first introduced into a 100-mL Parr reactor. The system was then purged with N_2, compressed to 300 psig and heated to 200°C. The feed – consisting of CPO, toluene (internal standard) and a designated water volume – was placed into a 30-mL feeding cylinder, pressurized to 800 psig and injected to the reactor when the set temperature was stabilized. The stirring speed remained at 750 rpm, but the reaction time varied among catalysts and was intentionally chosen to measure initial rates with conversions below 20%. These low conversions guaranteed that externally added water was significantly in excess relative to the *in situ* produced water. The post-reaction suspension was cooled down in an ice bath and centrifuged for 10 mins. The separated liquid was then analyzed by GC-FID.

2.1.3. Quantification of active sites under reaction conditions

Apart from CO_2-TPD, active sites of MgO catalysts were quantified via titration with propanoic acid, acting as a deactivating site titrant, following a recently described method,[51] in which propanoic acid was added to irreversibly block TiO_2 acid-base site pairs during acetone

self-condensation. This controlled site blockage helps quantifying the number of active sites on the catalyst surface. The operating temperature and initial cyclopentanone concentration were respectively fixed at 150°C and 1.8 M, while the mass of each catalyst and reaction time were adjusted for initial rate measurements. Propanoic acid was assumed to irreversibly block acid-base site pairs via monodentate mode; that is, one mole of acid was irreversibly adsorbed on one mole of Mg-O pairs. As the amount of propanoic acid in the feed was increased a corresponding suppression in aldol condensation rate was observed. Extrapolating the linear decline with acid uptake to zero rate (x-intercept) allows to determine the density of active sites, acid-base pairs titrated by propanoic acid, according to the expression:

$$\frac{V_{\text{propanoic acid adsorbed}} \times \rho^{150^{o}C}_{\text{propanoic acid}}}{MW_{\text{propanoic acid}} \times w_{\text{catalyst}}}$$

2.1.4. Water addition to the reaction mixture

For each MgO catalyst, a series of reactions were conducted at 200°C with increasing volumes of added water. Different amounts of water – 200 μL, 355 μL, 700 μL, 1000 μL and 1500 μL – were injected to the reactor to investigate the effects of water on catalytic activity. With a total reactor volume of 100 mL and 50 mL of reaction mixture, it can be calculated (See **Supporting Information A**) that addition of 355 μL results in the saturation of the gas phase with water vapor at 200°C. That is, with the first two injections, water remained in the vapor phase, while with the other injections a liquid aqueous phase was expected to form. \

2.2. Computational simulations

Ab initio molecular dynamics (AIMD) simulations were performed using Vienna *ab initio* simulation package (VASP).[52] The ion–electron interaction was described through the projector-augmented wave (PAW) approach.[53,54] For the structural optimization, the exchange and correlation energy was represented using the Perdew-Burke-Ernzerhof (PBE) functional of the generalized gradient approximation (GGA).[55] The van der Waals interaction has been taken into account through the Grimme's DFT-D3 semi-empirical method.[56] The supercell contained 4 layers of (2×2) MgO (100) surface, with the bottom two layers fixed at the bulk positions.

There were 2 OTS in the supercell corresponding to an OTS density of 2.9 per nm^2. The Brillouin zone was sampled using k-point of (2×2×1) centered at Γ. A 300 eV cutoff for the plane-wave basis set was used in the AIMD simulations, while 400 eV was used for DFT calculation of cyclopentanone adsorption at the interface. The AIMD simulations were performed at 300K in canonical ensembles. The time step was set to 0.5 fs.

The MgO catalyst in the calculations of activation barriers for CPO aldol condensation was modeled with a close-packed 3 × 3 MgO(100) slab, with four layers and 15 Å vacuum in the z-direction. The bottom two layers were fixed at their bulk position while the top two layers were allowed to relax in all optimizations. The 4 × 4 × 1 Monkhorst-pack k-point mesh was used to sample the first Brillouin zone. For each reaction path, the transition state search was performed using the dimer method,[57] with the initial guesses for the transition state structure and the reaction trajectory obtained through the nudged elastic band (NEB) method.[58]

3. Results and Discussion

3.1. Catalyst Characterization

3.1.1. Thermogravimetric Analysis (TGA)

The TGA in **Figure 1** shows two distinct mass losses from MgO(70)-OTS(30). The first loss, from 40°C to 200°C, is ascribed to the desorption of physisorbed water. The second one, from 250°C to around 400°C, results from the oxidation of the octadecyl groups in air. From quantification of evolved CO_2 and H_2O in this region and assuming that (i) Cl ligands have been fully hydrolyzed to OH and (ii) Si is retained on the surface during TGA, one can determine the original loading of OTS MgO(70)-OTS(30). The calculated value – approximately 12 wt.% (see **Supporting Information B**) – is lower than the nominal 30 wt.% placed in contact with MgO substrate during the impregnation. Clearly, a significant fraction of the OTS added to MgO-NC is not effectively anchored on the surface of MgO and is removed by the post-synthesis washes in ethanol and centrifugation. Nevertheless, the remaining alkylsilane molecules remain firmly anchored to the surface and are able to tolerate moderately high temperatures without decomposition, particularly in the absence of air.

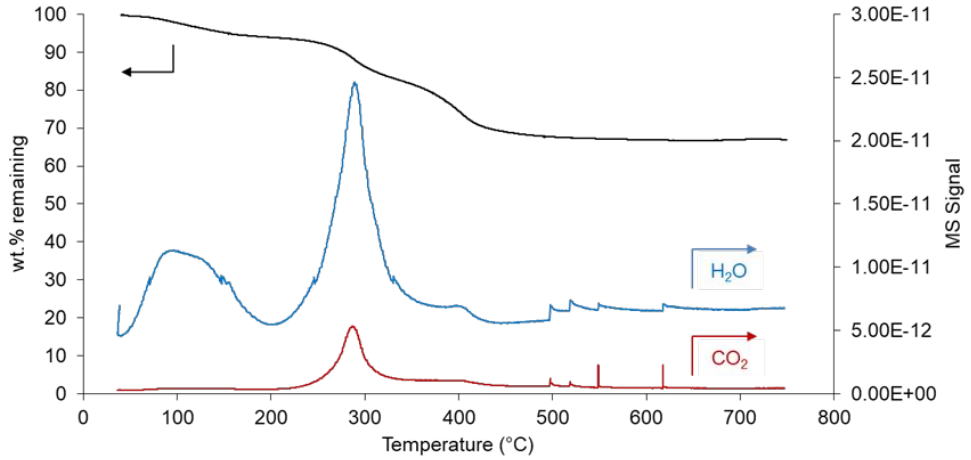

Figure 1. TGA and concurrent mass spectra of CO_2 and H_2O evolved from MgO(70)-OTS(30) during thermal oxidation.

3.1.2. Surface Area and Porosity

Table 1. Surface area, pore size and pore volume of various MgO catalysts.

Catalyst	S_{BET}	Pore size	Pore volume
	$m^2.g^{-1}$	nm	$cm^3.g^{-1}$
MgO-NC[19]	97	9.4	0.22
MgO(70)-OTS(30)[19]	51	3.8	0.04
MgO(70)-OTS(30) PC	61	13.1	0.19

Table 1 compares surface properties of the MgO-NC, MgO(70)-OTS(30) and MgO(70)-OTS(30) PC samples obtained by N_2 adsorption.

Using the values of OTS content in the MgO(70)-OTS(30) sample (as determined by TGA) and the BET surface area of MgO-NC into the equation in **Section 2.2.1**, we obtain approximately 3 molecules of OTS per nm^2 of MgO-NC, or as defined above x = 3 nm^{-2}. This OTS density is later used in the AIMD simulations, as discussed below. We can anticipate that

this high areal density of functional groups may impose steric constraints to the reaction. In fact, as shown below, we have found that these constraints may considerably limit the site-to-site access and therefore hinder the rate of bimolecular C-C coupling step.

If a uniform layer of anchored OTS on the surface of MgO is formed, one would expect that the average thickness of the OTS layer would be the difference between the radius of the pristine sample (4.7 nm) and that of the functionalized sample (1.9 nm). In fact, the resulting thickness (2.8 nm) is in good agreement with that estimated by Wang *et al.*[59] for the growth of ultrasmooth OTS layers on flat SiO_2 surfaces, 2.6 ± 0.2 nm.

By oxidatively removing the OTS functional groups from the MgO(70)-OTS(30) sample via temperature-programmed calcination, most of the pore volume and a fraction of the surface area of the original MgO-NC sample were recovered. That is, in the MgO(70)-OTS(30) PC sample the pores that were partially filled with the organic layers in the MgO(70)-OTS(30) were reopened as the alkyl chains of OTS were oxidized to gaseous CO_2 and H_2O, while the inorganic Si^{4+} cations remained chemically bonded to the MgO. This process is not reversible enough to regain all of the surface area of the original MgO and most importantly, as shown below, it significantly reduces its activity by neutralizing the most basic sites on the surface. However, as also inferred below from kinetic measurements, the steric constraints posed by the alkyl groups are readily removed.

3.1.3. CO_2-TPD for quantification of density and strength of basic sites

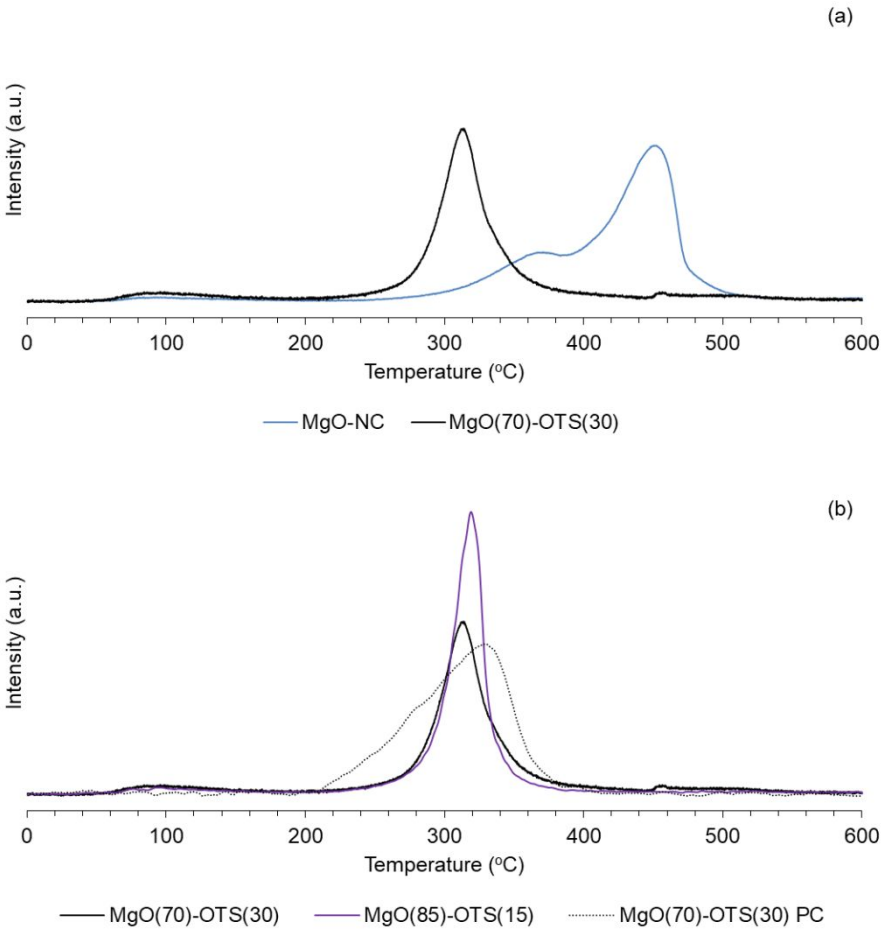

Figure 2. CO_2-TPD on directly OTS-functionalized MgO catalysts.

To quantify the density of basic sites on the as-prepared MgO catalysts, we used the conventional TPD of adsorbed CO_2, as shown in **Figure 2a.** The conventional MgO-NC exhibits two desorption peaks centered at 460 and 370 °C, typically ascribed to sites of strong and medium basicity. By contrast, the functionalized MgO(70)-OTS(30) shows a single peak centered at 320°C, which might be attributed to medium basic strength, with a clear removal of the high-temperature desorption peak, ascribed to strong basic sites.

A similar elimination of the high-temperature desorption peak upon functionalization was previously observed on MgO@mSiO$_2$-OTS samples.[19] The fact that the same changes

upon functionalization are observed with samples of different porosities and surface areas supports the notion that the disappearance of the high-temperature peak upon OTS grafting is due to the removal of the strongest basic sites, rather than to changes in physical structure (pore and surface area), which many times affect position of TPD peaks by transport and readsorption effects and may lead to erroneous conclusions.[60] In this case, it is reasonable to expect that if the pore size decreases with functionalization one would expect a delay in desorption if mass transport effects were dominant. However, the shift is in the other direction, which suggests that TPD is indeed probing basicity. Moreover, one can expect that the sites that more readily react with OTS during functionalization are those of higher basicity, for example those with lower coordination number, which are shown to disappear on the TPD of the functionalized sample. Therefore, it is reasonable to conclude that the active sites remaining on MgO(70)-OTS(30) are of weaker basicity than those on the parent MgO-NC.

Figure 2b compares the CO_2 TPDs of two additional samples with that of the functionalized MgO(70)-OTS(30). One of them, MgO(85)-OTS(15), contains a lower density of functional groups and the TPD indicates that the grafted amount is enough to neutralize all the strong basic sites, but less of the medium basicity, which were partially removed on the sample with higher OTS content. The other sample is the original MgO(70)-OTS(30) that has been dealkylated by calcination in air at 450^{o}C, indicated as a post-calcined sample, MgO(70)-OTS(30) PC. Interestingly, this sample still shows a peak centered at 320^{o}C, but broader. Since the high temperature peak is not recovered one can conclude that SiO_2 fragments remain chemisorbed on the strongest basic sites. Nevertheless, there is a noticeable increase in the total density of sites due the removal of the octadecyl groups, which might have been blocking accessible sites on the MgO(70)-OTS(30) sample.

3.2. Quantification of active sites under reaction conditions by titration

The active Mg-O sites were quantified via isothermal titration with propanoic acid, following Wang *et al.*,[51] who demonstrated that propanoic acid strongly blocks acid–base site pairs on TiO_2 during acetone condensation and allows a quantitative estimation of the total

number of these sites. In these measurements, we obtained initial rates of the self-condensation of CPO at 150°C, with varying amounts of propanoic acid in the feed. The amount of acid irreversibly adsorbed by MgO was calculated from the difference between the concentration in the feed and after exposure to the catalyst. The measured rate decreased proportionally to the amount of titrant propanoic acid adsorbed. Extrapolation to zero rate gives an estimate of the density of acid–base site pairs responsible for the CPO condensation activity.

Table 2. Intrinsic initial activities of CPO condensation on various MgO catalysts at 150°C.

Catalyst	**Intrinsic initial activity**
	$mmol.g^{-1}.h^{-1}$
MgO-NC	123
MgO(70)-OTS(30) PC	13
MgO(70)-OTS(30)	5

Table 2 summarizes intrinsic activities of the MgO catalysts obtained in the batch reactor at 150°C without addition of any propanoic acid. The rate per gram roughly follows the changes in surface area and overall density of basic sites obtained from CO_2-TPD. However, as shown below, the activity per site will be much higher for the non-functionalized MgO-NC catalyst, which has the strongest basicity.

Propanoic acid titration curves for the three samples, MgO-NC, MgO(70)-OTS(30) and MgO(70)-OTS(30) PC are shown in **Figure 3.** Since no traces of propanoic acid were detected by GC-FID analysis in any of the runs, we can safely conclude that it was irreversibly adsorbed on basic sites at all concentrations. The linearity of the data points corresponding to the runs on MgO(70)-OTS(30) and MgO(70)-OTS(30) PC would indicate that these catalysts have uniform active sites. From the extrapolations to zero rate, we can estimate densities of active sites of 295 and 330 $\mu mol.g^{-1}$ for MgO(70)-OTS(30) and MgO(70)-OTS(30) PC, respectively, two values that agree remarkably well with the basic site densities obtained by CO_2-TPD (**Table 3**).

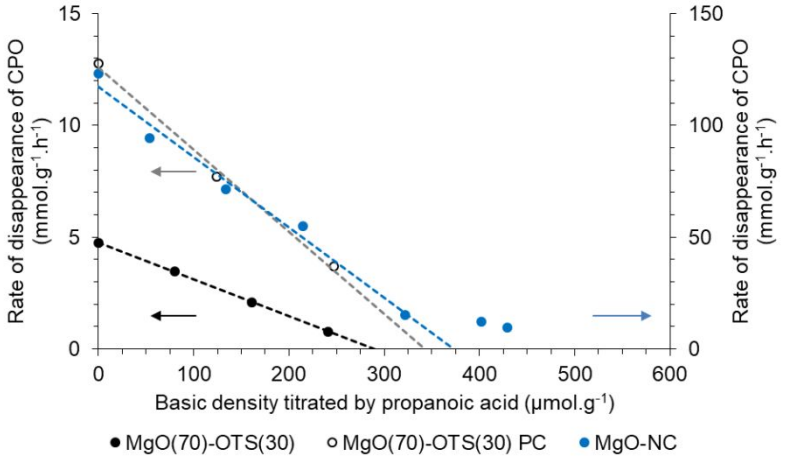

Figure 3. Propanoic acid-controlled aldol condensation rates on various MgO catalysts. Reaction conditions: $C_{CPO\,0}$ = 1.8 M, 150°C; 0.50 g of MgO-NC – 30 mins; 0.50 g of MgO(70)-OTS(30) – 4 hours; 0.325 g of MgO(70)-OTS(30) PC – 2 hours.

Contrary to the uniformly linear trend observed for the functionalized catalysts, the titration curve of MgO-NC shows two decreasing trends. The first linear drop extrapolates to a site density of 375 µmol.g^{-1}. Beyond this density, it seems to be another contribution of sites for which the decreasing slope is much lower. This overall non-linearity could be ascribed to presence of active sites with different basic strength, which is consistent with the CO_2-TPD result that shows at least two different types of sites. If that is the case, the first extrapolation would correspond to the density of strong basic sites and the second one to sites of medium strength. The approximate values obtained for each type (375 and 107 µmol.g^{-1}) are in reasonable agreement with the values obtained by TPD (317 and 102 µmol.g^{-1}).

Table 3. Densities of basic sites on various MgO-based catalysts.

Catalyst	CO_2-TPD		Propanoic acid titration	
	Strong sites	Medium sites	Strong sites	Medium sites
	μmol.g^{-1}	μmol.g^{-1}	μmol.g^{-1}	μmol.g^{-1}
MgO-NC	317	102	375	107
MgO(70)-OTS(30)	-	305	-	295
MgO(85)-OTS(15)	-	375	-	-
MgO(70)-OTS(30) PC	-	354	-	330

3.3. Effect of water addition on specific reaction rates

Figure 4 illustrates the contrasting behavior of the functionalized catalysts to that of the non-functionalized MgO-NC. In the absence of added water, not only they exhibit a very different specific rate, but also a distinct TOF, consistent with the presence of sites of varying basicity. Moreover, the effect of water addition is dramatically different for the functionalized compared to the non-functionalized catalyst. For MgO-NC, the rate drops sharply and consistently with increasing amount of added water, regardless of the state of water (vapor or liquid). This inhibition is ascribed to an active site blocking by water chemisorption competing with cyclopentanone at low water contents, and to the nucleation of a diffusion-limiting water film covering the surface as the amount of added water increases. Also, at high water contents, formation of an inactive $Mg(OH)_2$ layer leads to irreversible catalyst deactivation, observed in this catalyst.[19] By contrast, for the functionalized MgO(85)-OTS(15) and MgO(70)-OTS(30) catalysts, the activity increases with the presence of water vapor in the system until the partial pressure of water is high enough to start condensation at the reaction conditions. At this point the activity starts decreasing for all catalysts, which as described above may be due to the formation of a water film on the surface that causes mass transfer limitations. For the MgO(85)-OTS(15) catalyst, the observed rate-enhancement from no water added to 0.355 mL added is 42% and for the MgO(70)-OTS(30) sample is 140%.

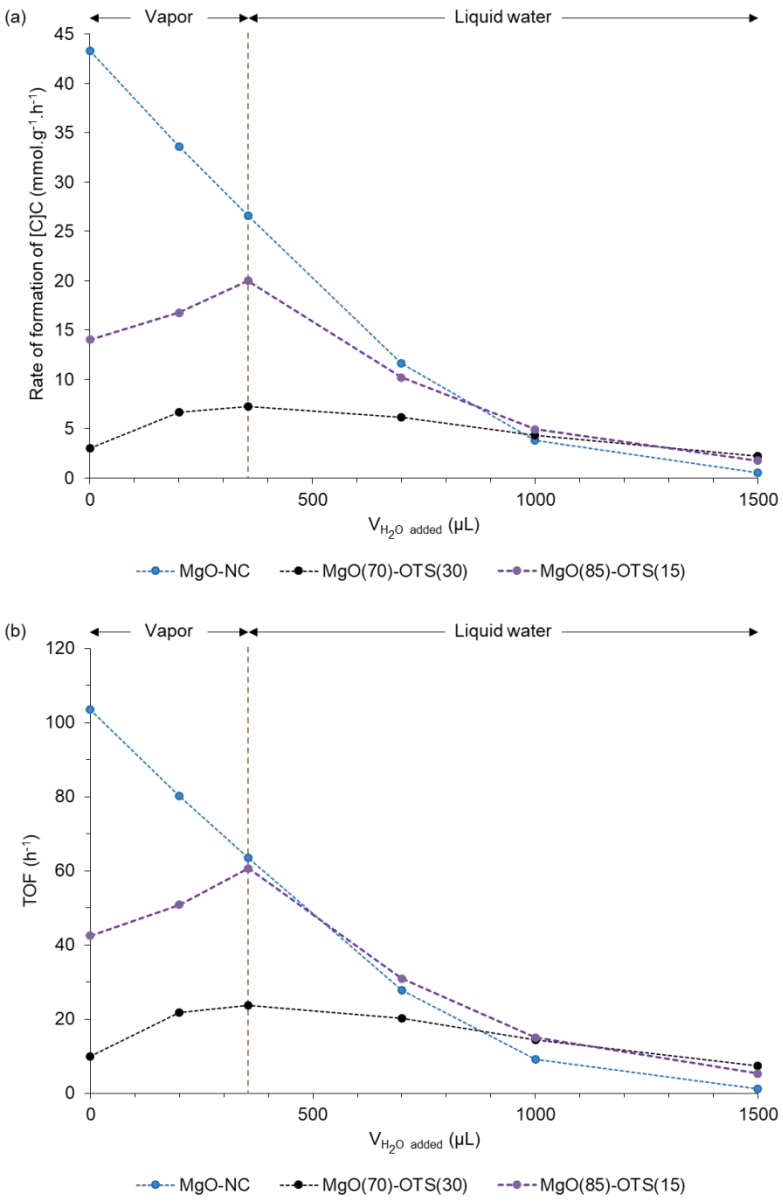

Figure 4. Effect of water addition on the catalytic performance of various MgO catalysts (a) Initial rate per gram of catalyst, (b) Initial rate per active site (TOF). Reaction conditions: $C_{CPO\,0}$ = 1.8 M, 200°C.

3.4. *Effect of the alkyl chain on the role of water*

To investigate whether the promoting effect of water is related to the elimination of the most active basic sites by the functionalization or the presence of the hydrophobic moieties, we quantified the effect of water addition onto the post-calcined sample MgO(70)-OTS(30) PC. As mentioned above, this sample keeps the most basic (active) sites blocked as the original functionalized sample, but its alkyl groups have been removed.

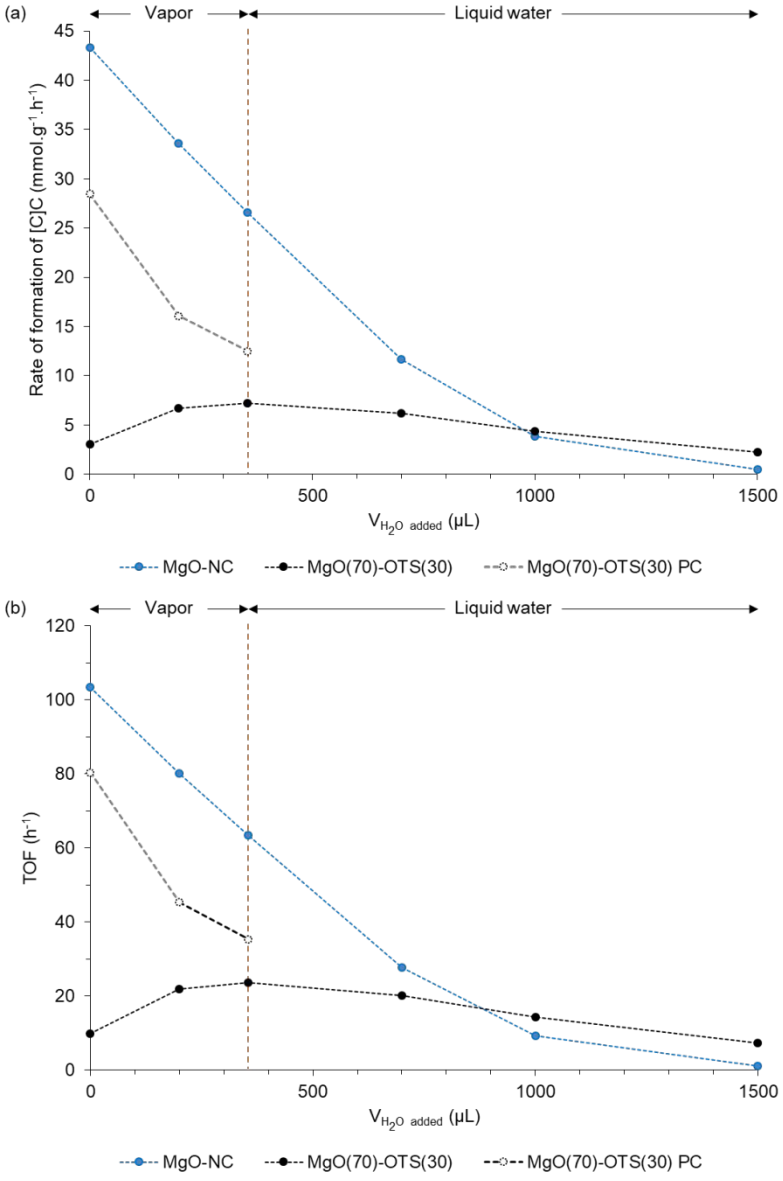

Figure 5. Effect of water addition on the catalytic performance post-calcined dealkylated MgO(70)-OTS(30) PC catalyst compared to the same sample before calcination and the non-functionalized MgO-NC. (a) Initial rate per gram of catalyst, (b) Initial rate per active site (TOF). Reaction conditions: $C_{CPO\,0}$ = 1.8 M, 200°C.

As shown in **Figure 5**, the activity of this sample decreases with the addition of water vapor, similar to the non-functionalized MgO-NC but contrary to the originally functionalized MgO(70)-OTS(30), which showed a clear enhancement in activity. This difference suggests that the promotion by water is related to the alkyl chains of the organosilane agent.

3.5. Reaction kinetics analysis

When working on a batch reactor, it is essential to decouple catalyst deactivation from the kinetics in the analysis of time evolution of concentration. The most effective method is measuring initial rates at varying initial concentrations. Therefore, separate 1-hour runs were conducted for each initial CPO concentration over MgO(70)-OTS(30) and MgO(70)-OTS(30) PC catalysts at 200°C. Initial rates over MgO-NC at 150°C, obtained on the same reaction system have been reported in previous work.[19]

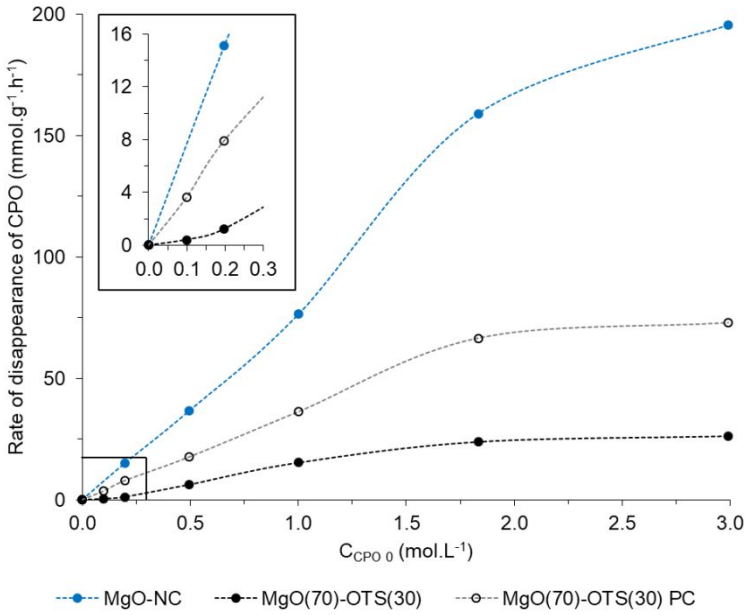

Figure 6. Initial rates of cyclopentanone (CPO) conversion over various MgO-based catalysts as a function of CPO concentration. Reaction conditions: 50 mL of total feed; MgO: 0.25 g - 150°C - 20 min reaction; MgO(70)-OTS(30): 0.50 g - 200°C - 1 hour reaction; MgO(70)-OTS(30) PC: 0.325 g - 200°C - 1 hour reaction. Inset: Expanded low CPO concentration region, emphasizing the differences in initial slopes.

Figure 6 compares initial rates over the three different MgO-based catalysts as a function of CPO initial concentration. The most important differences are observed in the low-concentration region (see inset). Clearly, the data for the non-functionalized MgO-NC and dealkylated MgO(70)-OTS(30) PC catalyst shows a first-order dependence (linear) while that of the functionalized MgO(70)-OTS(30) shows a second-order dependence (parabolic). Beyond 1.8 M the rates for all samples start plateauing as the surface coverage increases, typical of a Langmuir-Hinshelwood (L-H) kinetics. That is, the presence of the OTS alkyl groups on the surface not only improves the material stability in liquid water[19] but also changes the reaction kinetics due to a surface phenomenon that is discussed below.

Among the elementary steps of the solid base-catalyzed aldol-condensation mechanism, either the α-H abstraction[51] or the C-C coupling[61] has been proposed to be rate-limiting. While the former (also referred as deprotonation, enolate formation or α-H activation) responds to a first-order surface kinetics, the latter is intrinsically a second-order phenomenon. This step can follow either a bimolecular Langmuir-Hinshelwood (L-H) model between two surface species or an Eley-Rideal (E-R) model between an adsorbed enolate and an electrophile in the bulk.[19] In the **Supporting Information C** we include the details of the kinetics analysis, in which we tested the different models for each of the cases, either assuming first-order L-H (deprotonation), second-order L-H, or second-order E-R (C-C coupling) as rate-limiting steps.

Both, non-linear regressions and regressions using linearized L-H or E-R equations were used to compare the goodness of the fitting (See **Supporting Information D**). The analysis shows that for the non-functionalized MgO-NC catalyst the rate-limiting step is deprotonation following a first-order L-H model.

These kinetics results, obtained over the bare MgO catalyst, are in good agreement with the activation barriers for the two elementary steps of CPO aldol condensation calculated by DFT on the MgO(100) surface. As shown in **Figure 7**, starting with two CPO molecules adsorbed on a Lewis acid site (MgO), the barrier for the H-abstraction step that generates the enolate intermediate is 60 kJ/mol. This barrier is significantly higher than the one for the second step (C-C coupling). In this second step the enolate formed after H-abstraction attacks the other CPO molecule, which is adsorbed on an adjacent site and acts as the electrophile in the reaction. That is, the DFT calculations predict that the first-order H-abstraction step is rate-limiting, in good accord with the observed kinetics behavior.

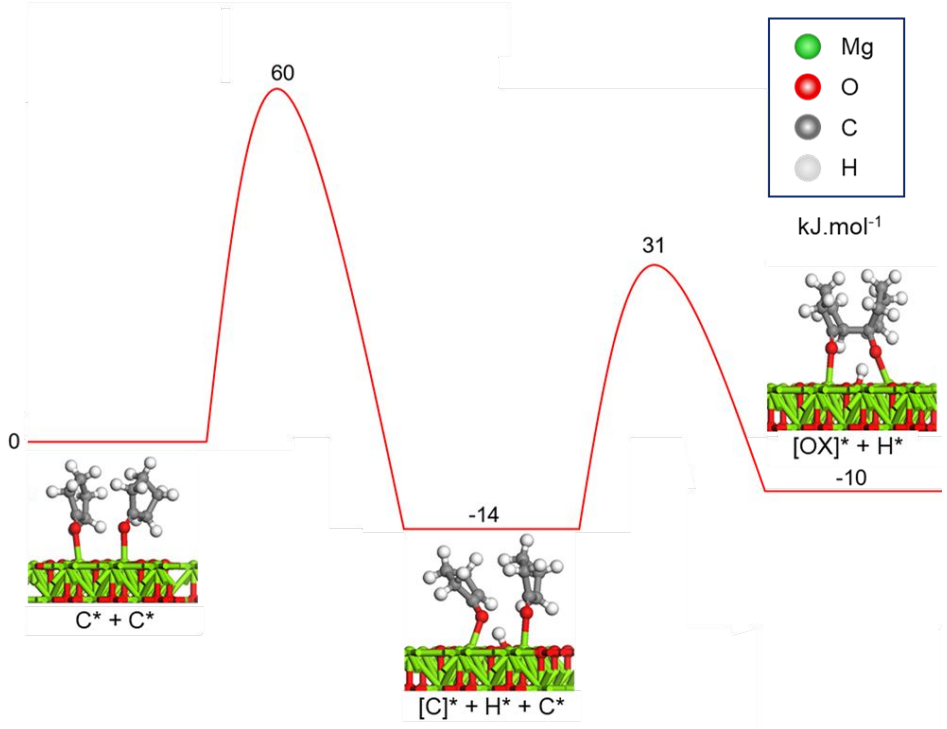

Figure 7. Energies of DFT-calculated reactant, transition state and product structures for the self-aldol condensation of cyclopentanone on a MgO(100) surface. In the first step, one of two cyclopentanone molecules adsorbed on adjacent Mg cations undergoes alpha H-abstraction by a basic site (oxygen). In the second step, the resulting enolate attacks the second cyclopentanone molecule, forming a new C-C bond.

By contrast, for the functionalized MgO(70)-OTS(30) catalyst, the best fitting corresponds to a second-order L-H model, which indicates that the surface C-C coupling is rate-limiting in this case. That is, the presence of the functional groups may put a steric constrain limiting the accessibility of the enolate to the carbonyl group of the adsorbed CPO, polarized by the Lewis acid site. In fact, it was further observed that when the alkyl chains of OTS molecules were removed, the resulting MgO(70)-OTS(30) PC catalyst behave very similarly to the non-functionalized MgO-NC. That is, the kinetics became again first-order L-H, indicating that the H-abstraction went back to be the rate-limiting step. Clearly, the cause for this switch in rate-limiting step can be traced to the presence of the alkyl groups on the surface, which play a steric constrain in the C-C coupling step.

3.5.1. Density Functional Theory simulation of cyclopentanone chemisorption on OTS-functionalized MgO

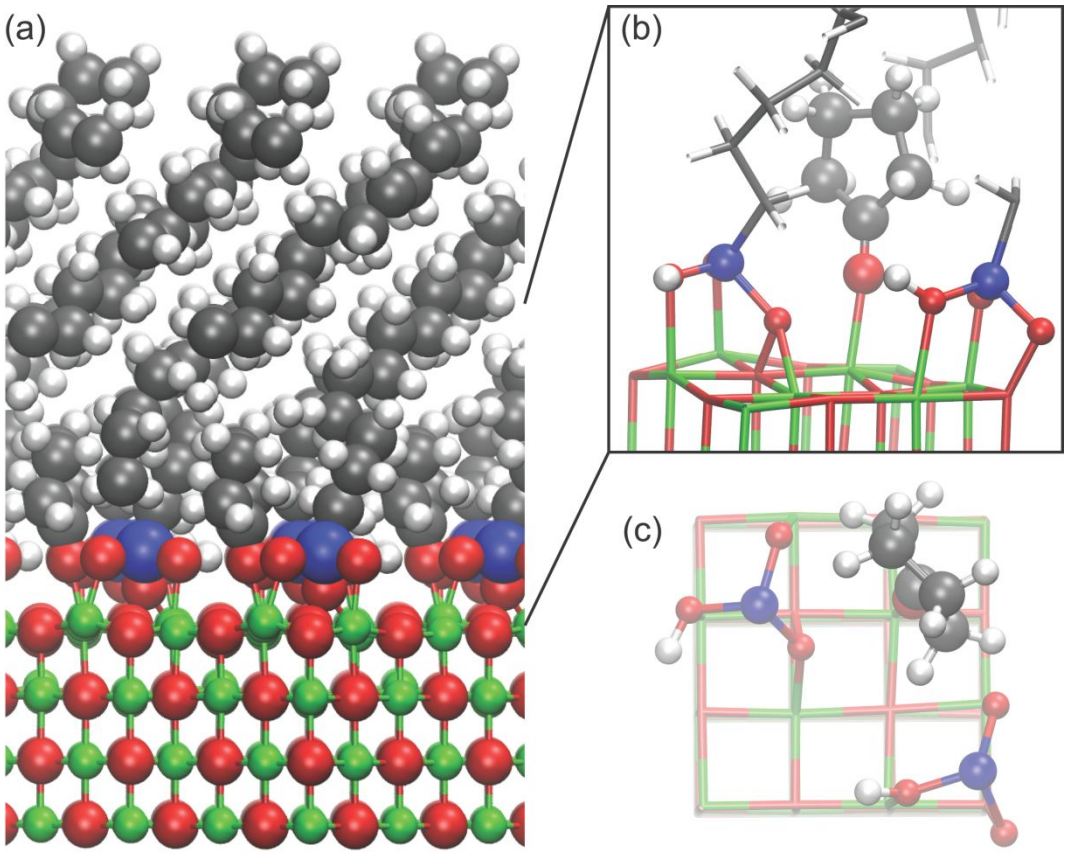

Figure 8. DFT calculations of the adsorption of CPO on OTS-functionalized MgO. (a) Atomic structure of the hybrid interface, with Mg, O, Si, C, and H colored pink, red, blue, cyan, and white, respectively. The OTS density in this simulation is about 3 molecules per nm^2, as observed experimentally. (b) Side view of the unit cell to show the adsorption configuration of CPO at the interface. (c) Top view of the unit cell. The carbon chain in the OTS has been omitted to show the densely packed interface.

We can rationalize this finding as follows. On the non-functionalized MgO catalyst, the C-C coupling is very effectively catalyzed by acid-base pairs,[51] in which the basic site is responsible for the α-H abstraction that generates the enolate while the acid site acts as a polarizing agent that enhances the electrophilicity of the C in the carbonyl of the electrophile. As a result, the rate-limiting step is the first-order deprotonation. The functionalization of the surface has two effects that inhibit the reaction. First, it preferentially removes the sites of strongest basicity, but more importantly for the MgO(70)-OTS(30) catalyst, it places a steric constraint making the C-C coupling between adjacent sites much less feasible. As a result, the overall rate drops and the C-C coupling becomes rate-limiting. In perfect agreement with this idea, when the functionalized sample is calcined, we observe that as the steric constraint is removed, the rate-limiting step is again the first-order deprotonation. However, since the most basic sites have been removed and not recovered after calcination, the overall TOF is lower than in the original non-functionalized catalyst.

Figure 8 shows the atomic structure of cyclopentanone adsorption at the OTS/MgO interface. The AIMD simulations were performed first to equilibrate the structures of the OTS/MgO over 30 ps at room temperature, and then a cyclopentanone molecule was introduced using one of the snapshots taken from the AIMD simulation. The OTS is anchored to the MgO surface through Si-O-Mg covalent bonds. In this case, we assume one silanol still remains per OTS at the interface. **Figure 8c** depicts an adsorbed cyclopentanone molecule along with 2 OTS anchors over an 8 Å x 8 Å unit cell, being equivalent to 3 OTS anchors per nm^2, as observed experimentally (see **Section 3.1.2**). Because of this high density of OTS on the MgO surface, adsorption of two cyclopentanone molecules in the close proximity is hindered, as

discussed above, which is crucial in determining the reaction kinetics and the observed changes in rate-limiting step.

We can now rationalize the contrasting responses of the functionalized and non-functionalized catalysts to the addition of water on the basis of the observed kinetics and the representation of the functionalized surface, as revealed by the DFT simulations. The effect of water on the non-functionalized MgO is clearly detrimental for activity, at all concentrations. The observed kinetics and high TOF observed on this catalyst indicate that the bimolecular C-C coupling step is very favorable on the available acid-base pair sites, and the overall rate is limited by the initial deprotonation step, which is favored by strong basic sites. Then, the detrimental effect of water may simply be due to the blocking of active sites, which is common in many reactions.

3.5.2. *Mechanistic aspects of the water-assisted C-C coupling*

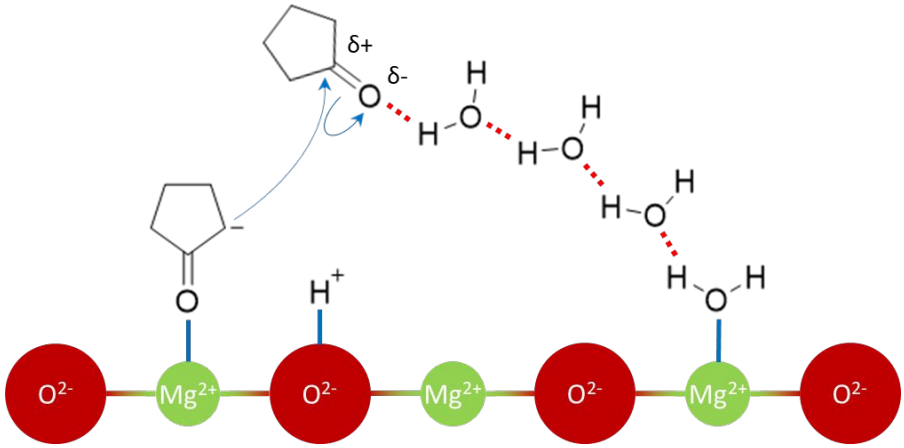

Figure 9. Schematic water-assisted C-C coupling as an elementary step of the nucleophilic addition mechanism of CPO self-aldol condensation.

What is less common is the significant enhancement in activity observed on the functionalized catalysts by the presence of water. Such enhancement must be traced to a phenomenon that accelerates the rate-limiting step, which in this case is the C-C coupling. As mentioned above, the reason for the reduced rate in the C-C coupling step is the presence of alkyl groups, which put a steric barrier between the surface enolate and the other CPO molecule acting as the electrophile. While the first CPO can still access the surface and get deprotonated by basic sites on MgO(70)-OTS(30), it becomes difficult for the resulting enolate to find adjacent surface-bound CPO molecules to attack. As illustrated in **Figure 8**, the alkyl groups of OTS also block the access of a neutral CPO molecule to an Mg^{2+} Lewis acid site, which normally would act as an enhancer of catalytic activity via polarization of the C=O bond. Particularly, the anionic α-C of a deprotonated cyclopentanone targets the carbonyl C of a neutral cyclopentanone molecule to form a new C-C bond. The more polar the neutral cyclopentanone C=O bond, the more electropositive the carbonyl C is to accelerate the nucleophilic attack of the α-C. As a consequence, C-C coupling replaces deprotonation as the rate-limiting step on MgO(70)-OTS(30).

From all of this, we must conclude that the presence of water somehow overcomes this steric constraint facilitating the rate-limiting C-C coupling. One may propose that clusters of

water molecules may nucleate around a Lewis acid site and extent the polarizing effect of this site to reach the carbonyl group of a CPO molecule next to the enolate, facilitating in this way the C-C coupling. As proposed in the schematic representation of **Figure 9,** external water can bridge the polarizing effect of a remote Lewis site via H-bonding to the carbonyl O of the CPO molecule. This polarization helps shifting the electron density in the carbonyl, rendering the C sufficiently electropositive to interact with the anionic α-C. From this perspective, water effectively shuttles the polarizing effect of remote Lewis sites onto the CPO molecules accessible to the surface enolate and accelerates the rate-limiting C-C coupling.

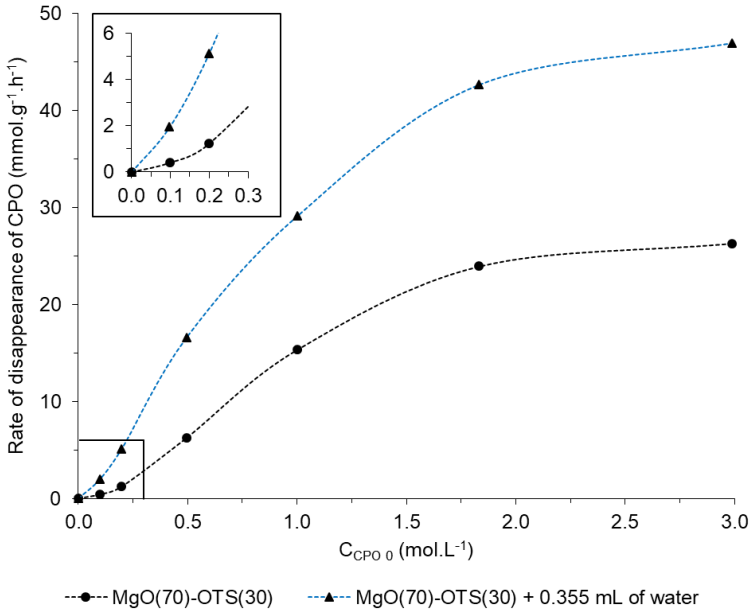

Figure 10. Initial rates of cyclopentanone (CPO) conversion over MgO(70)-OTS(30) as a function of CPO concentration - with and without externally added water. Reaction conditions: 50 mL of total feed, 0.50 g of MgO(70)-OTS(30), 200°C, 1 hour. Inset: Expanded low CPO concentration region, emphasizing the differences in initial slopes.

As shown in **Figure 10** and **Figure S4**, the rate can be well described by a second-order L-H model, which shows that C-C coupling remains being rate-limiting after water addition, but with an enhanced overall rate. The as-described water-induced rate-enhancement holds until a water film is formed over the surface, causing a drop in activity.

3.6. *Kinetic isotope effect by adding D_2O instead of H_2O*

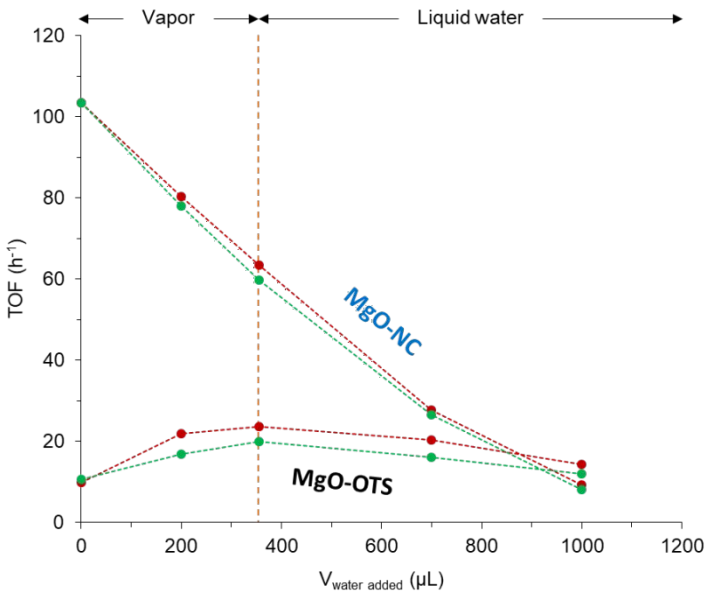

Figure 11. Effect of water addition - H_2O (red symbols); D_2O (green symbols) on the catalytic performance of non-functionalized and OTS-functionalized MgO catalysts. Reaction conditions: $C_{CPO\,0}$ = 1.8 M, 200°C.

Figure 11 displays changes in reaction rates when D_2O is added to the system instead of H_2O. A small, but consistent, isotope effect is observed on the OTS-functionalized MgO but almost no effect on the non-functionalized MgO-NC. As mentioned in **Section 3.5.2**, the rate-limiting step on the former is C-C coupling, which is positively affected by water. While the exact mechanism of polarization via H-bonding is beyond the scope of this study, it is clear that there is an effect of the nature of the water molecules, which is less pronounced with the heavier D atoms than with H. Meanwhile, on the non-functionalized MgO-NC, the rate-limiting step is deprotonation, which is negatively affected by water via blocking of active sites. In that sense H_2O and D_2O are comparable inhibitors.

4. Conclusions

The main conclusions of the study are the following:

i. As previously shown, functionalizing MgO with octadecyltrichlorosilane (OTS) improves the stability of this catalyst for aldol condensation of cyclopentanone, but at the same time it changes the rate-limiting step. That is, while on the non-functionalized MgO the reaction follows a first-order L-H model with α-H abstraction as rate-limiting step, it becomes second-order L-H, limited by C-C coupling and exhibits a lower TOF.

ii. The decreased catalytic activity of the MgO-OTS sample compared to MgO-NC can be partially recovered by adding moderate amounts of water to the reaction system. The promotional effect of external water relates to the alkyl chains of the organosilane agent.

iii. It is proposed that water assists the rate-limiting C-C coupling step by helping polarizing the C=O bond of the cyclopentanone molecule that acts as the electrophile. A chain of water molecules can form a bridge between an Mg^{2+} acid site and a cyclopentanone electrophile near the surface cyclopentenolate. In other words, a cyclopentanone molecule in the organic solvent can become indirectly polarized by the Mg^{2+} bridging the steric constraints imposed by the alkyl groups of the organosilane.

Acknowledgements

This material is based upon work supported by the U.S. Department of Energy, Office of Science, Basic Energy Sciences under Award Number DE-SC0018284. Experimental participation of the exchange student Gabriel Rocha (Brazil) is greatly acknowledged. The computational research used supercomputer resources at the National Energy Research Scientific Computing Center (NERSC) and the OU Supercomputing Center for Education & Research (OSCER) at the University of Oklahoma.

Supporting Information.

Estimation of the maximum water volume added to reaction system to keep water vapor; estimation of OTS content on OTS-functionalized MgO from TGA; identification of valid kinetic models by linear and non-linear fitting of experimental data with various kinetic models.

References

(1) Pham, T. N.; Shi, D; Resasco, D. E., Evaluating Strategies for Catalytic Upgrading of Pyrolysis Oil in Liquid Phase. *Appl. Catal., B* **2014**, *145*, 10–23.

(2) Herron, J. A.; Vann, T. S.; Duong, N. N.; Resasco, D. E.; Crossley, S. P.; Lobban, L. L.; Maravelias, C. T., A System-Level Roadmap for Biomass Thermal Fractionation and Catalytic Upgrading Strategies. *Energy Technology* **2017**, *5*(1), 130–150.

(3) Resasco, D. E.; Crossley, S. P., Implementation of Concepts Derived from Model Compound Studies in the Separation and Conversion of Bio-Oil to Fuel. *Catal. Today* **2015**, *257*, 185–199.

(4) Duong, N. N.; Wang, B.; Sooknoi, T.; Crossley, S. P.; Resasco, D. E., Enhancing the Acylation Activity of Acetic Acid By formation of an intermediate Aromatic Ester. *Chemsuschem* **2017**, *10*(13), 2823–2832.

(5) Resasco, D. E.; Wang, B.; Sabatini, D., Distributed Processes for Biomass Conversion Could Aid UN Sustainable Development Goals. *Nat. Catal.* **2018**, *1*, 731–735.

(6) Czernik, S.; Bridgwater, A. V., Overview of Applications of Biomass Fast Pyrolysis Oil. *Energy Fuels* **2004**, *18*, 590–598.

(7) Wilson, J.; Chen, E. Y., Organocatalytic Cross-Coupling of Biofuranics to Multifunctional Difuranic C_{11} Building Blocks. *ACS Sustainable Chem. Eng.* **2016**, *4*(9), 4927–4936.

(8) Konwar, L. J.; Samikannu, A.; Maki-Arvela, P.; Mikkola, J., Efficient C–C Coupling of Bio-Based Furanics and Carbonyl Compounds to Liquid Hydrocarbon Precursors Over Lignosulfonate Derived Acidic Carbocatalysts. *Catal. Sci. Technol.* **2018**, *8*, 2449–2459.

(9) Alonso, D. M.; Bond, J. Q.; Dumesic, J. A., Catalytic Conversion of Biomass to Biofuels. *Green Chem.* **2010**, *12*, 1493–1513.

(10) Wang, B.; Crossley, S. P.; Resasco, D. E., Zeolite-Catalysed C–C Bond Forming Reactions for Biomass Conversion to Fuels and Chemicals. *Catal. Sci. Technol.* **2016**, *6*, 2543–2559.

(11) Hronec, M.; Fulajtarova, K., Selective Transformation of Furfural to Cyclopentanone. *Catal. Commun.* **2012**, *24*, 100–104.

(12) Cueto, J.; Faba, L.; Diaz, E.; Ordonez, S., Cyclopentanone As an Alternative Linking Reactant for Heterogeneously Catalyzed Furfural Aldol Condensation. *Chemcatchem* **2017**, *9*, 1765–1770.

(13) Hasni, M.; Prado, G.; Rouchaud, J.; Grange, P.; Devillers, M.; Delsarte, S., Liquid Phase Aldol Condensation of Cyclopentanone With Valeraldehyde Catalysed By Oxynitrides Possessing Tuneable Acid–Base Properties. *J. Mol. Catal. A: Chem.* **2006**, *247*, 116–123.

(14) Yang, J.; Li, N.; Li, G.; Wang, W.; Wang, A.; Wang, X.; Cong, Y.; Zhang, T., Synthesis of Renewable High-Density Fuels Using Cyclopentanone Derived from Lignocellulose. *Chem. Commun.* **2014**, *50*, 2572–2574.

(15) Liang, D.; Li, G.; Liu, Y.; Wu, J.; Zhang, X., Controllable Self-Aldol Condensation of Cyclopentanone Over MgO-ZrO_2 Mixed Oxides: Origin of Activity & Selectivity. *Catal. Commun.* **2016**, *81*, 33–36.

(16) Di Cosimo, J. I.; Diez, V. K.; Ferretti, C.; Apesteguia, C. R., Basic Catalysis on MgO: Generation, Characterization and Catalytic Properties of Active Sites. *RSC Catal.* **2014**, *26*, 1–28.

(17) Merzhanov, A.; Borovinskaya, I.; Yukhvid, V.; Ratnikov, V. In *Scientific Principles of Material Science*, Nauka, Moscow, **1981**, P 193.

(18) Varma, A.; Rogachev, A.; Mukasyan, A.; Hwang, S., Combustion Synthesis of Advanced Materials: Principles and Applications. *Adv. Chem. Eng.* **1998**, *24*, 79–226.

(19) Ngo, D. T.; Sooknoi, T.; Resasco, D. E., Improving Stability of Cyclopentanone Aldol Condensation MgO-Based Catalysts by Surface Hydrophobization With Organosilanes. *Appl. Catal., B* **2018**, *237*, 835–843.

(20) Krishnamoorthy, S.; Tu, M.; Ojeda, M. P.; Pinna, D.; Iglesia, E., An Investigation of the Effects of Water on Rate and Selectivity for the Fischer–Tropsch Synthesis on Cobalt-Based Catalysts. *J. Catal.* **2002**, *211*, 422–423.

(21) Shi, D.; Faria, J.; Pham, T. N.; Resasco, D. E., Enhanced Activity and Selectivity of Fischer−Tropsch Synthesis Catalysts in Water/Oil Emulsions. *ACS Catal.* **2014**, *4*, 1944–1952.

(22) Michel, C.; Zaffran, J.; Ruppert, A.M.; Matras-Michalska, J.; Jedrzejczyk, M.; Grams, J.; Sautet, P., Role of Water in Metal Catalyst Performance for Ketone Hydrogenation: A Joint Experimental and Theoretical Study on Levulinic Acid Conversion into Gamma-Valerolactone. *Chem. Comm.*, **2014**, *50*, 12450-12453.

(23) Su, H.; Yang, M.; Bao, X.; Li, W., The Effect of Water on the CO Oxidation on Ag(111) and Au(111) Surfaces: A First-Principle Study. *J. Phys. Chem. C* **2008**, *112*, 17303–17310.

(24) De Wispelaere, K.; Hemelsoet, K.; Waroquier, M.; Van Speybroeck, V., Complete Low-Barrier Side-Chain Route for Olefin Formation During Methanol Conversion in H-SAPO-34. *J. Catal.* **2013**, *305*, 76–80.

(25) Ren, R.; Zhang, Y.; Liu, S.; Zuo, Z.; Lu, Y., DFT Studies of the Methanol Decomposition Mechanism on the H_2O/Cu(110) and OH Pre-Adsorbed H_2O/Cu(110) Interfaces: Comparison With the Clean Cu(110) Surface. *Int. J. Hydrogen Energy* **2016**, *41*, 2411–2423.

(26) Zhang, R.; Liu, H.; Wang, B.; Ling, L., Insights into the Preference of CO_2 Formation from HCOOH Decomposition on Pd Surface: A Theoretical Study. *J. Phys. Chem. C* **2012**, *116*, 22266–22280.

(27) Jekewitz, T.; Blickhan, N.; Endres, S.; Drochner, A.; Vogel, H., The Influence of Water on the Selective Oxidation of Acrolein to Acrylic Acid on Mo/V/W-Mixed Oxides. *Catal. Commun.* **2012**, *20*, 25–28.

(28) Ai, M., Oxidation of Propane Over V_2O_5–P_2O_5-Based Catalysts at Relatively Low Temperatures. *Catal. Today* **1998**, *42*, 297–301.

(29) Novakova, E. K.; Derouane, E. G.; Vedrine, J. C., Effect of Water on the Partial Oxidation of Propane to Acrylic and Acetic Acids on Mo-V-Sb-Nb Mixed Oxides. *Catal. Lett.* **2002**, *83*, 177–182.

(30) Petzold, T.; Blickhan, N.; Drochner, A.; Vogel, H., The Effect of Water on the Heterogeneously Catalyzed Selective Oxidation of Acrolein: An Isotope Study. *Chemcatchem* **2014**, *6*, 2053–2058.

(31) Chen, K.; Damron, J.; Pearson, C.; Resasco, D. E.; Zhang, L.; White, J. L., Zeolite Catalysis: Water Can Dramatically Increase or Suppress Alkane C–H Bond Activation. *ACS Catal.* **2014**, *4*, 3039–3044.

(32) Rytter, E.; Holmen, A., On the Support in Cobalt Fischer–Tropsch Synthesis – Emphasis on Alumina and Aluminates. *Catal. Today* **2016**, *275*, 11–19.

(33) Rytter, E.; Holmen, A., Perspectives on the Effect of Water in Cobalt Fischer−Tropsch Synthesis. *ACS Catal.* **2017**, *7*, 5321–5328.

(34) Li, J.; Jacobs, G.; Das, T. K.; Davis, B. H., Fischer–Tropsch Synthesis: Effect of Water on the Catalytic Properties of A Ruthenium Promoted Co/TiO_2 Catalyst. *Appl. Catal., A* **2002**, *233*, 255–262.

(35) Jimenez-Barrera, E.; Bazin, P.; Lopez-Cartes, C.; Romero-Sarria, F.; Daturi, M.; Odriozola, J. A., CO/H_2 Adsorption on A Ru/Al_2O_3 Model Catalyst for Fischer–Trospch: Effect of Water Concentration on the Surface Species. *Appl. Catal., B* **2018**, *237*, 986–995.

(36) Du Toit, E.; Nicol, W., The Rate Inhibiting Effect of Water as a Product on Reactions Catalysed By Cation Exchange Resins: Formation of Mesityl Oxide From Acetone As Case Study. *Appl. Catal., A* **2004**, *277*, 219–225.

(37) Bolt, P. H.; Habraken, F. H. P. M.; Geus, J. W., Formation of Nickel, Cobalt, Copper, and Iron Aluminates From *A*- and *Γ*-Alumina-Supported Oxides: A Comparative Study. *J. Solid State Chem.* **1998**, *135*, 59–69.

(38) Chen, J.; Wang, X.; Xiang, H.; Sun, Y., Study on Stability of $Co/ZrO_2/SiO_2$ Catalyst for Fischer–Tropsch Synthesis. *Stud. Surf. Sci. Catal.* **2001**, *136*, 525–529.

(39) Chen, J.; Xiang, H.; Gao, H.; Sun, Y., Study on Deactivation of $Co/ZrO_2/SiO_2$ Catalyst for Fischer–Tropsch Synthesis. *React. Kinet. Catal. Lett.* **2001**, *73*, 169–177.

(40) Van Steen, E.; Claeys, M.; Dry, M. E.; Van De Loosdrecht, J.; Viljoen, E. L.; Visagie, J. L., Stability of Nanocrystals: Thermodynamic Analysis of Oxidation and Re-Reduction of Cobalt in Water/Hydrogen Mixtures. *J. Phys. Chem. B* **2005**, *109*, 3575–3577.

(41) Zhang, L.; Chen, K.; Chen, B.; White, J. L.; Resasco, D. E., Factors that Determine Zeolite Stability in Hot Liquid Water. *J. Am. Chem. Soc.* **2015**, *137*, 11810–11819.

(42) Donnelly, T. J.; Satterfield, C. N., Product Distributions of the Fischer–Tropsch Synthesis on Precipitated Iron Catalysts. *Appl. Catal., A* **1989**, *52*, 93–114.

(43) Bukur, D. B.; Patel, S. A.; Lang, X., Fixed Bed and Slurry Reactor Studies of Fischer–Tropsch Synthesis on Precipitated Iron Catalyst. *Appl. Catal., A* **1990**, 61, 329–349.

(44) Wang, Y.; Zhu, X.; Crocker, M.; Chen, B.; Shi, C., A Comparative Study of the Catalytic Oxidation of HCHO and CO Over $Mn_{0.75}Co_{2.25}O_4$ Catalyst: The Effect of Moisture. *Appl. Catal., B* **2014**, *160-161*, 542–551.

(45) Saleh-Alhamed, Y. A.; Hudgins, R. R.; Silveston, P. L., Role of Water Vapor in the Partial Oxidation of Propene, *J. Catal.* **1996**, *161*, 430–440.

(46) Bu, W.; Zhao, L.; Zhang, Z.; Zhang, X.; Gao, J.; Xu, C., Effect of Water on Hydrogenation of 1,3-Butadiene Over Au(111): A Joint Theoretical and Experimental Study. *Appl. Surf. Sci.* **2014**, *289*, 6–13.

(47) Chen, K.; Kelsey, J.; White, J. L.; Zhang, L.; Resasco, D. E., Water Interactions in Zeolite Catalysts and their Hydrophobically Modified Analogues. *ACS Catal.* **2015**, *5*, 7480–7487.

(48) Henderson, M. A., The Interaction of Water With Solid Surfaces: Fundamental Aspects Revisited. *Surf. Sci. Rep.* **2002**, *46*, 1–308.

(49) Zapata, P. A.; Huang, Y.; Gonzalez-Borja, M. A.; Resasco, D. E., Silylated Hydrophobic Zeolites With Enhanced Tolerance to Hot Liquid Water. *J. Catal.* **2013**, *308*, 82–97.

(50) Pham, T. N.; Zhang, L.; Shi, D.; Komarneni, M. R.; Pilar Ruiz, M.; Resasco, D. E.; Faria, J., Fine–Tuning the Acid–Base Properties of Boron–Doped Magnesium Oxide Catalyst for the Selective Aldol Condensation. *Chemcatchem* **2016**, *8*, 3611–3620.

(51) Wang, S.; Goulas, K.; Iglesia, E., Condensation and Esterification Reactions of Alkanals, Alkanones, and Alkanols on TiO_2: Elementary Steps, Site Requirements, and Synergistic Effects of Bifunctional Strategies. *J. Catal.* **2016**, *340*, 302–320.

(52) Kresse, G.; Furthmuller, Efficient Iterative Schemes for *Ab Initio* Total-Energy Calculations Using A Plane-Wave Basis Set. *J. Phys. Rev. B* **1996**, *54*(16), 11169–11186.

(53) Blochl, P. E., Projector Augmented-Wave Method. *Phys. Rev. B* **1994**, *50*(24), 17953–17979.

(54) Kresse, G.; Joubert, D., From Ultrasoft Pseudopotentials to the Projector Augmented-Wave Method. *Phys. Rev. B* **1999**, *59*(3), 1758–1775.

(55) Perdew, J. P.; Burke, K.; Ernzerhof, M., Generalized Gradient Approximation Made Simple. *Phys. Rev. Lett.* **1996**, *77*(18), 3865–3868.

(56) Grimme, S.; Antony, J.; Ehrlich, S.; Krieg, H., A Consistent and Accurate *Ab Initio* Parametrization of Density Functional Dispersion Correction (DFT-D) for the 94 Elements H–Pu. *J. Chem. Phys.* **2010**, *132*(15), 154104–154122.

(57) Henkelman, G.; Jonsson, H. A Dimer Method for Finding Saddle Points on High Dimensional Potential Surfaces Using only First Derivatives. *J Chem Phys* 111, 7010-7022 (1999).

(58) Henkelman, G., Uberuaga, B. P., Jonsson, H. A Climbing Image Nudged Elastic Band Method for Finding Saddle Points and Minimum Energy Paths. *J Chem Phys* 113, 9901-9904 (2000).

(59) Wang, Y.; Lieberman, M., Growth of Ultrasmooth Octadecyltrichlorosilane Self-Assembled Monolayers on SiO_2. *Langmuir* **2003**, *19*, 1159–1167.

(60) Gorte, R. J., What Do We Know About the Acidity of Solid Acids? *Catal. Lett.* **1999**, *62*, 1–13.

(61) Shylesh, S.; Kim, D.; Gokhale, A.; Canlas, C.; Struppe, J.; Ho, C.; Jadhav, D.; Yeh, A.; Bell, A., Effects of Composition and Structure of Mg/Al Oxides on their Activity and Selectivity for the Condensation of Methyl Ketones. *Ind. Eng. Chem. Res.* **2016**, *55*, 10635–10644.